The Journal of Immunology

RIPK3–MLKL–Mediated Neutrophil Death Requires Concurrent Activation of Fibroblast Activation Protein- α

Xiaoliang Wang, Francois Gessier, Remo Perozzo, Darko Stojkov, Aref Hosseini, Keyvan Amirshahrokhi, Stefan Kuchen, Shida Yousefi, Pius Lötscher and Hans-Uwe Simon

J Immunol published online 12 August 2020
http://www.jimmunol.org/content/early/2020/08/11/jimmunol.2000113

Supplementary Material **http://www.jimmunol.org/content/suppl/2020/08/11/jimmunol.2000113.DCSupplemental**

The Journal of Immunology is published twice each month by
The American Association of Immunologists, Inc.,
1451 Rockville Pike, Suite 650, Rockville, MD 20852

Print ISSN: 0022-1767 Online ISSN: 1550-6606.

Published August 12, 2020, doi:10.4049/jimmunol.2000113

RIPK3–MLKL–Mediated Neutrophil Death Requires Concurrent Activation of Fibroblast Activation Protein-α

Xiaoliang Wang,* Francois Gessier,† Remo Perozzo,‡,1 Darko Stojkov,* Aref Hosseini,* Keyvan Amirshahrokhi,*,§ Stefan Kuchen,¶ Shida Yousefi,* Pius Lötscher,† and Hans-Uwe Simon*,‖

Cytokine-primed neutrophils can undergo a nonapoptotic type of cell death using components of the necroptotic pathway, including receptor-interacting protein kinase-3 (RIPK3), mixed lineage kinase-like (MLKL) and NADPH oxidase. In this report, we provide evidence for a potential role of serine proteases in CD44-mediated necroptotic death of GM-CSF–primed human neutrophils. Specifically, we observed that several inhibitors known to block the enzymatic function of fibroblast activation protein-α (FAP-α) were able to block CD44-mediated reactive oxygen species production and cell death, but not FAS receptor–mediated apoptosis. To understand how FAP-α is involved in this nonapoptotic death pathway, we performed immunoblotting experiments in the presence and absence of inhibitors of RIPK3, MLKL, p38 MAPK, PI3K, and FAP-α. The results of these experiments suggested that FAP-α is active in parallel with RIPK3, MLKL, and p38 MAPK activation but proximal to PI3K and NADPH oxidase activation. Interestingly, neutrophils isolated from the joints of patients suffering from rheumatoid arthritis underwent a GM-CSF–independent necroptosis following CD44 ligation; this effect was also blocked by both FAP-α and MLKL inhibitors. Taken together, our evidence shows that the RIPK3–MLKL pathway activates NADPH oxidase but requires, in addition to p38 MAPK and PI3K, a serine protease activity, whereby FAP-α is the most likely candidate. Thus, FAP-α could be a potential drug target in neutrophilic inflammatory responses to avoid exaggerated nonapoptotic neutrophil death, leading to tissue damage. ***The Journal of Immunology*****, 2020, 205: 000–000.**

Neutrophils are equipped with granules filled with reactive chemicals and enzymes and play an essential role in innate immunity (1–5). Neutrophil death, such as apoptosis and necroptosis, could influence the surrounding environment and inflammatory responses. Neutrophil apoptosis represents the most common form of both physiological and pathological cell death and is considered to be an option for limiting tissue damage by preventing the release of histotoxic contents from dying cells (5–7). Neutrophil necroptosis is a regulated form of necrosis, which is dependent on receptor-interacting protein kinase-3 (RIPK3) and mixed lineage kinase-like (MLKL) activities (5). Necroptotic neutrophils may induce inflammatory responses by the immediate release of danger-associated molecular patterns and also by causing tissue damage (5, 7). Thus, neutrophil necroptosis is considered highly detrimental to the resolution of inflammation owing to the consequent release of toxic cellular contents and the potential escape of pathogens into surrounding tissues (5, 7). Understanding the molecular mechanism of the necroptotic neutrophil death pathway may provide specific targets for potential therapeutic intervention in infectious, inflammatory, and autoimmune diseases (5).

Serine proteases constitute almost one third of all proteases and are characterized by a catalytic serine residue at the active site. They have been shown to play essential roles in biological processes in blood coagulation, development, signal transduction, immune response, inflammation, and cell death (3, 8–11). Fibroblast activation protein-α (FAP-α) is a serine protease belonging to the dipeptidyl peptidase (DPP) IV (CD26) gene family, also known as the S9b family (12–15), which is a subfamily of the prolyl-oligopeptidase family within the serine protease clan SC (16, 17). Apart from FAP-α, the DPP4 gene family includes DPP4, DPP8, DPP9, DPP-6 (also known as DPP4-like protein-1) and DPP10 (also known as DPP4-like protein-2) (16–18). DPP4 is the most extensively studied member of the DPP4 gene family and well known for its role in glucose homeostasis. It has become a validated therapeutic target for the treatment of type 2 diabetes (14, 18, 19). In contrast, FAP-α has been described to be highly

*Institute of Pharmacology, University of Bern, CH-3010 Bern, Switzerland; †Novartis Institutes for BioMedical Research, CH-4056 Basel, Switzerland; ‡School of Pharmaceutical Sciences, School of Pharmacy Geneva-Lausanne, University of Geneva, 1211 Geneva, Switzerland; §Department of Pharmacology, School of Pharmacy, Ardabil University of Medical Sciences, 561893141 Ardabil, Iran; ¶Department of Rheumatology, Clinical Immunology and Allergology, Inselspital, Bern University Hospital, University of Bern, CH-3012 Bern, Switzerland; and ‖Department of Clinical Immunology and Allergology, Sechenov University, 119991 Moscow, Russia

[1]Deceased.

ORCIDs: 0000-0002-6021-6116 (X.W.); 0000-0003-3251-9715 (F.G.); 0000-0001-6761-1736 (K.A.); 0000-0002-9855-4305 (S.Y.); 0000-0002-9404-7736 (H.-U.S.).

Received for publication January 31, 2020. Accepted for publication July 21, 2020.

This work was supported by Swiss National Science Foundation Grant 310030_184816 (to H.-U.S.).

X.W. conceived, planned and performed the study, analyzed and interpreted data, and wrote the paper. F.G. and P.L. synthesized and characterized pharmacological inhibitors. R.P., K.A., D.S., A.H., and S.Y. performed experiments; S.K. took clinical care of the rheumatoid arthritis patients and provided clinical material; and H.-U.S. provided overall guidance, experimental advice, laboratory infrastructure, and edited the paper. All authors read and approved the final manuscript.

Address correspondence and reprint requests to Dr. Hans-Uwe Simon, Institute of Pharmacology, University of Bern, Inselspital, INO-F, CH-3010 Bern, Switzerland. E-mail address: hus@pki.unibe.ch

The online version of this article contains supplemental material.

Abbreviations used in this article: DHR, dihydrorhodamine 123; DPI, diphenylene iodonium; DPP, dipeptidyl peptidase; FAP-α, fibroblast activation protein-α; GaM, goat anti-mouse; MLKL, mixed lineage kinase-like; NOX, NADPH oxidase; PIP3, PI(3,4,5)P3; p-MK2, phospho-Thr334-MK2; RA, rheumatoid arthritis; RIPK3, receptor-interacting protein kinase-3; ROS, reactive oxygen species; TPCK, *N*-p-tosyl-l-phenylalanine chloromethyl ketone.

expressed in cancer stroma cells and plays a role in tumor growth and metastasis (15, 19, 20). It should be noted, however, that talabostat, an FAP-α inhibitor, showed only minimal or no clinical anticancer effects in clinical trials (19, 21–23).

FAP-α, also referred to as seprase, is structurally homologous to DPP4, sharing 52% amino acid sequence identity (15, 16) and is the most similar family member to DPP4 (24). *FAP-α* and *DPP4* genes contain both 26 exons, are located adjacent to each other, and have similar gene sizes of 72.8 and 81.8 kb, respectively, all of which suggest they represent a product of gene duplication (16, 17). FAP-α and DPP4 share a similar catalytic region with comparable enzymatic activity (17); however, FAP-α has not only a DPP activity but also exhibits endopeptidase activity, enabling it to cleave gelatin, collagen type I, and α_2-antiplasmin, which makes it distinct from other members of the DPP4 gene family (15, 20). Besides soluble forms (15, 20, 25, 26), FAP-α can also be expressed as a 95-kDa type II integral membrane glycoprotein, forming 170-kDa homodimers (14, 16, 27). Although FAP-α is not expressed or is difficult to detect in most normal human tissues (15, 20), low levels of both mRNA and protein expression have been found in skin, breast tissue, endometrium, cervix, pancreas, and placenta (17, 28). In contrast, high FAP-α expression is found in embryonic tissues or at pathologic sites, including cancer, wound healing, atherosclerosis, liver and lung fibrosis, tumor-associated macrophages, arthritis, or inflammation (15, 17, 20, 29). Because of its unique expression pattern, FAP-α has been emerging as a potential drug target in recent years (15, 17).

A nonapoptotic death under in vitro conditions can be mediated in cytokine-primed human neutrophils following ligation of surface adhesion receptors, such as CD44 (30, 31), CD11b (31), CD18 (31), or CD15 (31). Moreover, evidence was obtained that such regulated necrotic neutrophil death occurs in some inflammatory diseases (5, 30–33). This neutrophil death pathway requires RIPK3–MLKL signaling, which together with p38 MAPK and PI3K activates the NADPH oxidase (NOX) (31). In the present report, we provide evidence that FAP-α is activated in parallel with RIPK3–MLKL–p38 MAPK signaling and is involved in the activation of NOX in CD44-activated and cytokine-primed human neutrophils, leading to nonapoptotic cell death.

Materials and Methods

Reagents

Anti–FAP-α mAb (clone 1E5), anti-CD44 mAb (clone A3D8), *N*-p-tosyl-L-phenylalanine chloromethyl ketone (TPCK), and dihydrorhodamine 123 (DHR) were purchased from Sigma-Aldrich (Buchs, Switzerland). The $F(ab')_2$ fragments of the secondary goat anti-mouse (GaM) Ab were purchased from Jackson ImmunoResearch (Milan Analytica; Roche Diagnostics, Rotkreuz, Switzerland). GM-CSF was supplied by Novartis (Nuremberg, Germany). PMA was purchased from Calbiochem (VWR, Dietikon, Switzerland). Wortmannin and diphenylene iodonium (DPI) chloride were purchased from Calbiochem-Novabiochem (La Jolla, CA). Q-VD-OPh was from SM Biochemicals (Anaheim, CA). Anti-DPP4 mAb (clone 9F1.2) and PD169316 were obtained from Merck Millipore (Darmstadt, Deutschland). Anti-FAS agonistic mAb (CH11) was purchased from MBL International (Woburn, MA). GSK′843 was from Glixx Laboratories (Southborough, MA), and GW806742X was from Adipogen AG (Liestal, Switzerland). Rabbit anti–phospho-Ser473-AKT, rabbit anti-p38, rabbit anti–phospho-Thr334-MK2 (p-MK2), and rabbit anti–phospho-Thr180/Tyr182-p38 Abs were from Cell Signaling Technology (Danvers, MA). Anti-GAPDH mAb was obtained from Chemicon International (Chandlers Ford, U.K.). HRP-coupled secondary Abs (anti-mouse IgG and anti-rabbit IgG) were from GE Healthcare (VWR). Luminata Forte Western HRP substrate was purchased from Millipore (Billerica, MA). Talabostat was from MedChemExpress (Lucerna-Chem AG, Lucerne, Switzerland). The pseudopeptide inhibitor M83 (catalog number: CS16989; sequence: acetyl-Arg-AEEA-(D)Ala-(L)boroPro.) was purchased from CSBio (Menlo Park, CA). FAP 293T Cell Transient Overexpression Lysate (Denatured) (catalog number: H00002191-T01) and FAP MaxPab rabbit polyclonal anti–FAP-α Ab (D01) (catalog number: H00002191-D01) were ordered from Abnova (Lucerna-Chem AG). KE-86-QG38 (patent: Novartis AG; Novartis Pharma GmbH WO2007/113226, 2007, A1; location in patent: Page/Page column 133–135), alogliptin, and saxagliptin were synthesized in the Novartis Institutes for BioMedical Research (Basel, Switzerland) (Supplemental Fig. 1). The characterization of their inhibitory activity is shown in Table I. The calpain I, caspase-3/7, caspase-8, as well as the proteasome chymotrypsin and the proteasome trypsin bioluminescent assay kits were from Promega AG (Duubendorf, Switzerland). The EnzChek Elastase Assay Kit (E-12056), the specific elastase inhibitor *N*-methoxy succinyl-Ala-Ala-Pro-Val-chloromethyl ketone, and the elastase inhibitor IV (127373-66-4) were from Thermo Fisher Scientific (Waltham, MA.). PI3K Activity ELISA: Pico (K-1000s) and PI3K α (p110α/p85α) active enzyme (E-2000) were from Echelon Biosciences (Salt Lake City, UT). The SensoLyte 520 Cathepsin D Fluorimetric Assay Kit was purchased from AnaSpec (Fremont, CA). Purified α-chymotrypsin and trypsin enzymes from bovine pancreas, GW311616A, E-64 (L-transepoxysuccinyl-leucylamido-[4-guanidino] butane), calpastatin peptide (208902), PMSF, pepstatin A, BSA (A-7906), and aprotinin were purchased from Sigma-Aldrich. Recombinant human caspase-3 (BML-SE169), caspase-8 (BML-SE172), and PI-103 (ALX-270-460-M001) were from Enzo Life Sciences AG (Lausen, Switzerland). Recombinant human calpain I (208713) was purchased from Merck KGaA (Schaffhausen, Switzerland). Recombinant human FAP-α was obtained from R&D Systems and Bio-Techne (Abingdon, U.K.). FAP-α substrate (Z-Gly-Pro-AMC) was from Bachem Holding AG (Bubendorf, Switzerland). The mouse anti-human CD63 mAb (clone H5C6) was from BD Biosciences (Allschwil, Switzerland), and mouse anti-human CD16 (clone DJ130c) from Santa Cruz Biotechnology (Dallas, TX).

Cells

Peripheral blood neutrophils from healthy normal individuals and patients suffering from rheumatoid arthritis (RA) associated with acute joint inflammation were purified by Ficoll-Hypaque centrifugation as described previously (30–32). Joint fluid neutrophils from patients with RA were also isolated, using the same protocol as described previously (32). The purity of the isolated human neutrophil populations was always >95% as assessed by staining with Diff-Quik (Baxter Diagnostics, Düdingen, Switzerland) followed by light microscopic analysis.

Immature neutrophils were isolated from bone marrow aspirates as previously described (34). PBMCs were separated from peripheral blood of healthy normal individuals by Ficoll-Hypaque density gradient centrifugation as described previously (35, 36). Written informed consent was obtained from all blood and bone marrow donors, and the study was approved by the Ethics Committee of Canton Bern.

HT-29 and Caco-2 cancer cells were obtained from the American Type Culture Collection (Manassas, VA).

Cell cultures

Human blood neutrophils were cultured at 1×10^6/ml in RPMI 1640 medium plus GlutaMAX (Invitrogen) supplemented with 5% FCS (endotoxin <1 endotoxin unit/ml) and antibiotics in the presence or absence of GM-CSF (10 ng/ml), anti-FAS (1 μg/ml), PMA (25 nM), Q-VD-OPh (10 or 20 μM), PD169316 (10 μM), wortmannin (100 nM), DPI (1 μM), GSK′843 (50 μM), GW806742X (5 μM), TPCK (10 or 20 μM), talabostat (50 μM), KE-86-QG38 (10 μM), alogliptin (10 or 50 μM), saxagliptin (10 or 50 μM), or M83 (1, 10, 50, 100, 200, 500, or 1000 μM). Preincubation with inhibitors for 30 min and subsequent GM-CSF priming for another 30 min were performed before ligation of CD44. Anti-CD44 mAb (6 μg/ml) was added for 15 min prior to addition of GaM (20 μg/ml) for receptor ligation. Cells were cultured for the indicated time periods in a humidified 37°C incubator at 5% CO_2.

HT-29 and Caco-2 cancer cells were cultured in DMEM plus GlutaMAX (Invitrogen) supplemented with 10% FCS and antibiotics. Cells were kept in a humidified 37°C incubator at 5% CO_2.

Determination of cell death

Cell death was assessed by uptake of 25 μM ethidium bromide followed by flow cytometric analysis (FACSCalibur; BD Biosciences) (31, 37).

Oxidative burst measurements

Oxidative burst measurements in human neutrophils were performed using fluorescent detection of reactive oxygen species (ROS) activity by flow cytometry. One hundred microliters of neutrophils (1×10^6/ml) were cultured as indicated and subsequently incubated with 1 μM DHR 123 at 37°C for 30 min. The reaction was stopped by adding 100 μl of ice-cold

PBS placed on ice, and then the ROS activity of the samples was immediately measured by flow cytometry (FACSCalibur) (30, 31, 38).

For time-course of oxidative burst measurements, 100 μl of neutrophils (1×10^6/ml) were cultured as indicated in black, glass-bottom, 96-well plates (Greiner Bio-One GmbH, Frickenhausen, Germany), and subsequently, 1 μM DHR 123 was added to each well. Fluorescent activity was immediately measured at an excitation of 485 nm and fluorescence emission intensity of 538 nm using a spectrofluorometer (SpectraMax M2; Molecular Devices, Biberach an der Riss, Germany). The kinetics of ROS production were time dependently analyzed every 5 min at 37°C up to 1 h. Relative DHR 123 fluorescence was obtained after subtraction of the corresponding DHR 123 fluorescence of medium without cells at the corresponding time point and subsequent norming of the values to initially measured fluorescence (39). PMA-stimulated cells served as positive controls.

Quantitative real-time PCR

Total RNA of cells was isolated using a commercially available kit from Zymo Research (Quick-RNA MicropPrep Kit; Lucerna-Chem AG) according to the technical manual provided. RNA was reverse transcribed to cDNA, and real-time PCR was performed using the iTaq Universal SYBR Green Supermix (Bio-Rad Laboratories AG, Cressier, Switzerland) with a real-time PCR machine (CFX Connect Real-Time PCR Detection system; Bio-Rad Laboratories). The primers used were as follows: human *DPP4*, 5′-AAA GGC ACC TGG GAA GTC ATC G-3′ and 5′-CAG CTC ACA ACT GAG GCA TGT C-3′; human *18S*, 5′-ATC CCT GAA AAG TTC CAG CA-3′ and 5′-CCC TCT TGG TGA GGT CAA TG-3′ (Microsynth AG, Balgach, Switzerland); the human *FAP-α* primer pair was ordered from Bio-Rad Laboratories AG (assay identification: qHsaCID0018575). The relative gene expression was measured by subtracting the cycle threshold (C_t) value of the target (*DPP4* and *FAP-α*) and control (*18S*) genes in the samples relative to the PBMC by the $2^{-\Delta\Delta Ct}$ method.

Immunoblotting

Immunoblotting experiments were performed as previously described (30, 31, 37). Briefly, human neutrophils were lysed in Triton lysis buffer (1% Triton X-100, 150 mM NaCl, 50 mM Tris-HCl [pH 7.4], and 1 mM EDTA) containing both protease (protease inhibitor mixture P8340 and PMSF; Sigma-Aldrich) and phosphatase inhibitors (1 μM okadaic acid, 1 mM Na_3VO_4, and 5 mM NaF). The lysates were heated at 95°C for 5 min. Proteins were separated by SDS-PAGE and electroblotted onto polyvinylidene difluoride membranes (Immobilion-P; Millipore, Bedford, MA). The membranes were routinely blocked in TBS containing 0.1% Tween 20 and 5% nonfat dry milk, followed by incubation overnight with the indicated Abs at 4°C. The next morning, samples were further incubated with the appropriate HRP-conjugated secondary Ab for 1 h at room temperature. Filters were developed according to the manufacturer's instructions (ECL Western Blotting Analysis System; GE Healthcare, Luminata Forte, Merck Millipore).

Calpain I activity assay

Human calpain I was diluted in 10 mM HEPES (pH 7.2) buffer containing 10 mM DTT, 1 mM EDTA, plus 0.1% BSA as a carrier, and used at 50 nM per reaction. The inhibitor E-64 (1 μM), *N*-acetyl-calpastatin peptide (5 μM), or KE-86-QG38 (1, 5, 10, and 20 μM) were incubated with the prediluted calpain I enzyme at room temperature for 5 min. Enzymatic activity of the calpain I was measured using a Calpain-Glo Kit (Promega AG) according to the instructions of the manufacturer. Ten minutes after addition of the Calpain-Glo reagent, luminescence was recorded as relative light units on a GloMax 96 Microplate Luminometer (Promega AG).

Caspase-3/7 and caspase-8 activity assays

Caspase-Glo 8 and Caspase-Glo 3/7 Assay Kits (Promega AG) were used according to the manufacturer's instructions. Purified recombinant caspase enzymes were diluted to 10 U/ml in 10 mM HEPES buffer containing 0.1% BSA as a carrier, and 50 μl of diluted caspases were preincubated with 0.5 μl of prediluted KE-86-QG38 (1, 5, 10, and 20 μM) or Q-VD-Oph (10 μM) in a white-walled 96-well plate (CELLSTAR Cell Culture Microplates, catalog number 655073; Greiner Bio-One) at room temperature for 5 min. Caspase-Glo Assay Reagent buffer was added up to a total volume of 100 μl and then incubated at room temperature for 20 min in the dark. The luminescence was recorded as relative light units on a GloMax 96 Microplate Luminometer (Promega AG).

Trypsin and α-chymotrypsin activity assays

Purified bovine pancreas trypsin or α-chymotrypsin were diluted to 1 μg/ml in 10 mM HEPES buffer (pH 7.6) and 50 μl of preincubated at room temperature for 5 min in the presence or absence of PMSF (10 μM for α-chymotrypsin), aprotinin (10 μM for trypsin), or KE-86-QG38 (1, 5, 10, and 20 μM) in a white-walled 96-well plate (CELLSTAR Cell Culture Microplates, catalog number 655073; Greiner Bio-One). Equal volume of Proteasome-Glo reagent was added to each well according to the instructions of the Proteasome-Glo 3-Substrate Cell-Based Assay System Kit. Luminescence was monitored after 20 min on a GloMax 96 Microplate Luminometer (Promega AG). The enzyme assay used Proteasome-Glo chymotrypsin-like assay (Suc-LLVY-Glo) and Proteasome-Glo trypsin-like assay (Z-LRR-Glo) substrates, respectively.

Cathepsin D activity assay

Enzymatic activity of cathepsin D was obtained using an enzyme-specific kit and performed according to the manufacturer's instructions (AnaSpec). The SensoLyte 520 Cathepsin D Activity Assay Kit uses a long wavelength Forster resonance energy transfer substrate based on a sequence surrounding the cleavage site of cathepsin D. When active cathepsin D cleaves the Forster resonance energy transfer substrate, it results in an increase of HiLyte Fluor 488 fluorescence monitored at excitation/emission of 490 nm/520 nm. Cathepsin D activity (fluorescence released by cleavage, HiLyte Fluor488) was assayed in a black, flat-bottom 96-well plate with nonbinding surface (Immuno Standard Modules, MaxiSorp, black, catalog number 475515; Thermo Fisher Scientific) in the presence or absence of the inhibitors KE-86-QG38 (1, 5, 10, and 20 μM), alogliptin (10 μM), or pepstatin A (1 μM) at room temperature for 5 min with a spectrofluorometer (SpectraMax M2).

Elastase activity assay

Elastase activity was measured using the EnzChek Elastase Assay Kit (E-12056; Thermo Fisher Scientific). The enzyme was prediluted and preincubated with GW311616A (10 μM), elastase inhibitor IV (127373-66-4) (10 μM), *N*-methoxy succinyl-Ala-Ala-Pro-Val-chloromethyl ketone peptide (10 μM; included in the kit), or KE-86-QG38 (1, 5, 10, and 20 μM) at room temperature for 5 min in a black, flat-bottom 96-well plate with a nonbinding surface (Immuno Standard Modules, MaxiSorp, black, catalog number 475515; Thermo Fisher Scientific) according to the manufacturer's instructions. Fluorescence was measured with a spectrofluorometer (SpectraMax M2; excitation at 485 nm and emission detection at 530 nm).

FAP-α activity assay

The enzyme assay was carried out in a black, flat-bottom 96-well plate (Immuno Standard Modules, MaxiSorp, black, catalog number 475515; Thermo Fisher Scientific) with the fluorescent FAP-α substrate (Z-Gly-Pro-AMC) at a final concentration of 50 μM in a buffer containing 50 mM Tris, 1 M NaCl, and 1 mg/ml BSA (pH 7.5). KE-86-QG38 (1, 5, 10, and 20 μM), alogliptin (10 μM), saxagliptin (10 μM), wortmannin (100 nM), or TPCK (20 μM) were preincubated at room temperature for 5 min before addition of the substrate to the wells. Fifty microliters of substrate was added to 50 μl of FAP-α enzyme (0.01 μg) per well, and the fluorescence was monitored every 2 min for 10 min with a spectrofluorometer (SpectraMax M2; excitation 380 nm and emission detection at 460 nm).

PI3K activity assay

The PI3K activity was determined using a PI3K ELISA Kit according to manufacturer's instructions (Echelon Biosciences). Purified PI3K α (p110α/p85α) active enzyme (Echelon Biosciences) was used to convert PIP2 substrate to PI(3,4,5)P3 (PIP3) in a kinase reaction and assessed by measuring the generated PIP3 by competitive ELISA. Preincubation of inhibitors, such as PI-103 (1 μM), wortmannin (10, 50, 100, and 200 nM), or KE-86-QG38 (1, 5, 10, and 20 μM), with PI3K enzyme was performed at room temperature for 5 min in KBZ buffer (included in the kit) prior to addition of PI(4,5)P2 substrate. After the PI3K reactions were completed, reaction products were first mixed and incubated with a PIP3 detector protein, then added to the PIP3-coated detection plate for competitive binding. A peroxidase-linked secondary detector was employed, and colorimetric reaction was detected at 450-nm absorbance on a plate reader (SpectraMax M2) to detect PIP3 detector binding to the plate. The colorimetric signal is inversely proportional to the amount of PIP3 produced by PI3K. PI3K activity was analyzed by comparing the absorbance values from the wells containing enzyme reaction products to the values in the PIP3 standard curve. PI3K activity in each sample was determined by the percentage conversion from initial 100 pmol of PI(4,5)P2 per assay point.

Immunofluorescence

Purified blood neutrophils were seeded on glass coverslips, fixed with 4% paraformaldehyde at room temperature for 10 min, and washed with PBS.

Following permeabilization with 0.05% saponin, cells were again washed with PBS, incubated in ice-cold acetone for 15 min at −20°C, and washed with PBS. Immunofluorescent staining was performed as previously reported (39). Briefly, samples were incubated in blocking buffer (2.5 mg/ml human Igs, 2.5 mg/ml normal goat serum, 2.5 mg/ml BSA in PBS) at room temperature for 1 h, and indirect immunostaining was performed using rabbit anti-human FAP-α polyclonal Ab (1:250) and mouse anti-CD16 mAb (1:250) or mouse anti-CD63 mAb (1:250). After overnight incubation with primary Abs at 4°C, samples were washed with PBS and incubated with Alexa Fluor 555–conjugated GaM and Alexa Fluor 488–conjugated goat anti-rabbit secondary Abs (Thermo Fisher Scientific; distributed by LuBioScience GmbH, Lucerne, Switzerland; both 1:400) in the dark at room temperature for 1 h and then analyzed with a confocal laser scanning microscope (LSM 700; Carl Zeiss Microimaging).

Statistics

Statistical analysis was performed using the Student *t* test. The figures show mean ± SEM. One-way ANOVA followed by a Tukey multiple comparisons test or the Kruskal–Wallis test followed by Dunn was applied for multiple comparisons. All p values <0.05 were considered as statistically significant.

Results

FAP-α activity is required for CD44-induced necroptosis in GM-CSF–primed human neutrophils

Serine proteases have been reported to be involved in the regulation of apoptotic and nonapoptotic types of neutrophil death (3, 40, 41). To test whether serine proteases are involved in RIPK3–MLKL–mediated neutrophil necroptosis, we ligated CD44 in GM-CSF–primed human neutrophils as previously described (30, 31), and observed that TPCK, a broad-spectrum pharmacological serine protease inhibitor, blocked cell death in this model (Fig. 1A), pointing to the possibility that serine proteases are involved in the death pathway. Serine proteases encoded by the DPP4 gene family and unrelated DPP4-like enzymes have been implicated in many physiological and pathological processes of the immune system (16, 19). Therefore, we tested several serine protease inhibitors of the DPP4 family (Supplemental Fig. 1) for their ability to block CD44-mediated neutrophil death. KE-86-QG38, able to block both FAP-α and DPP4 activities (Table I), inhibited CD44-induced neutrophil death in a concentration-dependent manner (Fig. 1B). In contrast, two known DPP4 inhibitors, alogliptin (42) and saxagliptin (43) (Table I), had no effect in this system, implying that DPP4 plays no role in this death pathway (Fig. 1C). As saxagliptin additionally exhibits anti-DPP8 and anti-DPP9 activities (Table I), it is also unlikely that DPP8 and DPP9 are involved in CD44-triggered neutrophil death. In contrast, talabostat, another DPP4 gene family protease inhibitor known to block FAP-α activity (19, 21–23), inhibited CD44-induced neutrophil death (Fig. 1C). Furthermore, M83, a pseudopeptide inhibitor with dual FAP-α and prolyl endopeptidase inhibitory effects (25, 44), at high concentrations also reduced CD44-triggered cell death (Fig. 1D). Taken together, KE-86-QG38, talabostat, and M83, which all block FAP-α activity, are able to inhibit CD44-induced neutrophil death. In contrast, blocking DPP4 activity had no effect in this system. It should be noted that both KE-86-QG38 and talabostat were unable to block FAS receptor–mediated apoptosis (Supplemental Fig. 2A). KE-86-QG38 and TPCK had also no effect on GM-CSF–mediated neutrophil survival (Supplemental Fig. 2B).

To exclude the possibility that KE-86-QG38 might mediate its effects in a FAP-α–independent manner, we further explored the characteristics of KE-86-QG38 by investigating its effect on the enzymatic activities of other proteases known to be expressed in human neutrophils, such as α-chymotrypsin, trypsin, caspase-3, caspase-8, calpain I, cathepsin D, and elastase. Our data showed that KE-86-QG38 is unable to inhibit these enzymes (Supplemental Fig. 3), further suggesting that it indeed inhibits CD44-induced neutrophil death by blocking FAP-α.

FAP-α is expressed in mature human neutrophils

We next investigated FAP-α and DPP4 expression in mature human neutrophils. As assessed by quantitative PCR and immunoblot analyses, we obtained evidence for FAP-α (Fig. 2A, 2C) but not for DPP4 expression (Fig. 2B, 2D). *FAP-α* mRNA expression was expressed at a lower level in immature as compared with mature neutrophils (Fig. 2A), suggesting that it is induced during neutrophil differentiation. Although we always observed FAP-α expression in mature human neutrophils, the expression varied among different blood donors (Fig. 2A, 2C). Besides neutrophils, we also observed FAP-α expression in human PBMC (Fig. 2A, 2C, right panel). Moreover, we used 293T cells overexpressing FAP-α and HT-29 cancer cells (45) as positive controls (Fig. 2A, 2C). In contrast, the levels of DPP4 mRNA in neutrophils were low as compared with PBMC and Caco-2 cancer cells (Fig. 2B) (46–48). Moreover, we were unable to detect DPP4 protein in neutrophils, whereas Caco-2 cancer cells were positive (Fig. 2D) (46). These data on DPP4 expression are in agreement with previously published work, which reported no detectable levels of DPP4 in mature human neutrophils (19).

We observed FAP-α expression in inflammatory neutrophils derived from joint fluid of RA patients. A cleaved fragment of FAP-α was more commonly expressed in this study as compared with control neutrophils (Fig. 2C, 2E). The observation of a cleaved FAP-α fragment is in agreement with previously published work (49, 50). It may represent a soluble form of FAP-α, which has been described to be located in the cytoplasm (15, 20, 25, 26). Indeed, we obtained evidence for FAP-α expression in close proximity to CD16, a surface molecule on neutrophils, and in the cytoplasm in close proximity to CD63, a molecule known to be associated with azurophilic granules (Fig. 2F) (51).

Because of the different expression of FAP-α expression in mature human neutrophils among different blood donors (Fig. 2A, 2C), we asked the question whether FAP-α levels determine the efficacy of CD44-mediated cell death. Although we observed a trend of more cell death induction after 24 h in FAP-α–high-expressing neutrophils compared with neutrophils with lower expression levels, this difference was NS (28.2 ± 7.0% as compared with 17.7 ± 5.5%). Moreover, we tested whether GM-CSF was able to induce the expression of FAP-α mRNA or protein in neutrophils in 3-h cultures and observed no significant differences (Supplemental Fig. 4).

Taken together, FAP-α but not DPP4 is expressed in mature human neutrophils, a finding which is consistent with the pharmacological data that pointed to a possible role for FAP-α in CD44-triggered neutrophil death in GM-CSF–primed neutrophils.

FAP-α activity is required for CD44-triggered ROS production in GM-CSF–primed human neutrophils

NOX-dependent ROS production has been shown to be critical for CD44-triggered neutrophil necroptosis (30, 31). To explore whether FAP-α activity is required either proximally or distally to NOX activation, we measured ROS production in activated neutrophils in the presence or absence of FAP-α inhibitors. Pharmacological inhibition of FAP-α by KE-86-QG38 or talabostat blocked CD44-triggered ROS production (Fig. 3A). In contrast, the DPP4 inhibitors alogliptin and saxagliptin had no effect on ROS production (Fig. 3A). TPCK also blocked ROS production, and DPI was used as positive control. In agreement with our previously published work, GW806742X, an MLKL inhibitor, PD169316, a p38 MAPK inhibitor, and wortmannin, a PI3K inhibitor, also

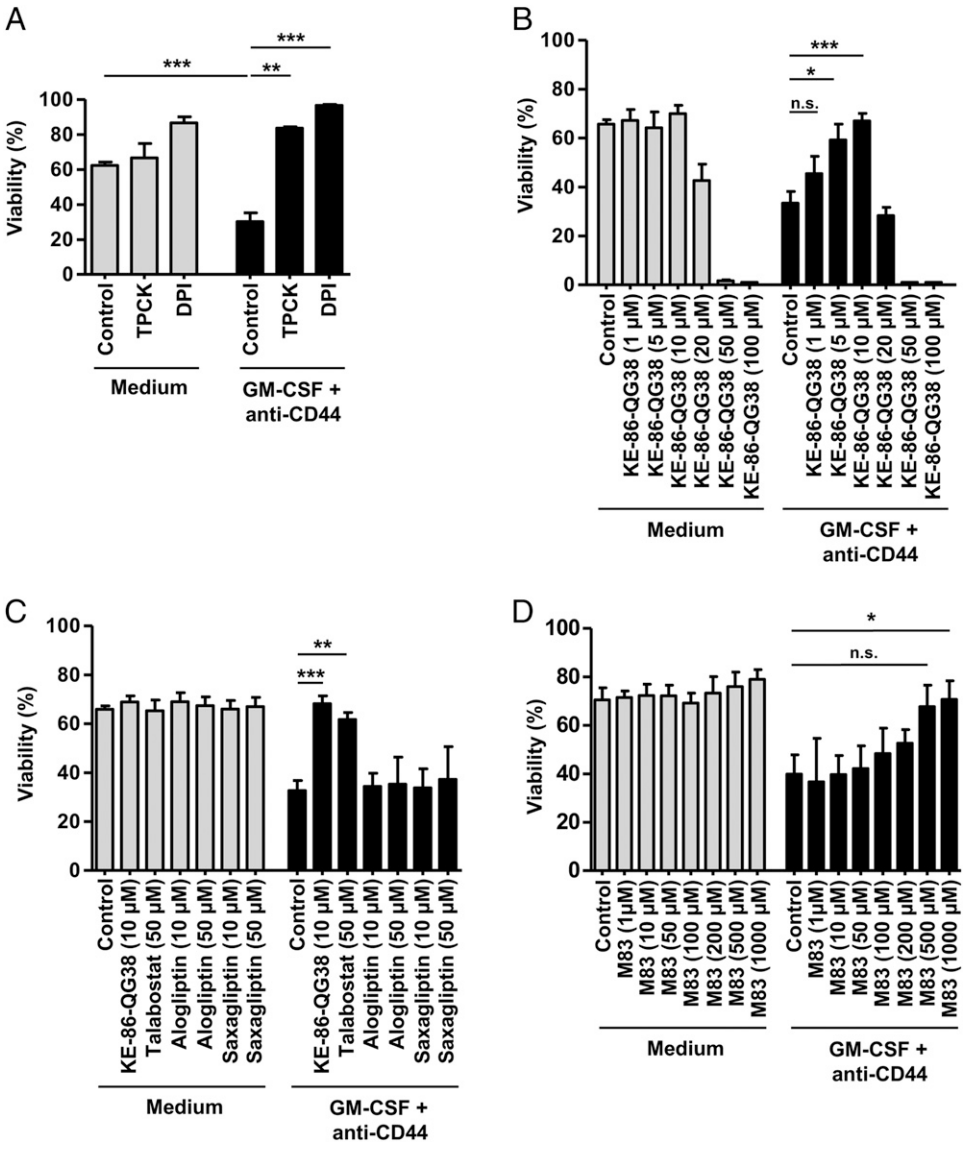

FIGURE 1. Enzymatic inhibition of FAP-α prevents CD44-triggered cell death in GM-CSF–primed human neutrophils. (**A**) Viability assay. Resting and activated neutrophils were cultured in the presence and absence of TPCK (10 μM) and DPI (1 μM). Neutrophils were cultured for 24 h before cell death analysis. All values are mean ± SEM ($n \geq 3$). $^{**}p < 0.01$, $^{***}p < 0.001$. (**B**) Viability assay. Resting and activated neutrophils were cultured in the presence and absence of KE-86-QG38 (1, 5, 10, 20, 50, or 100 μM). Neutrophils were cultured for 24 h before cell death analysis. All values are mean ± SEM ($n \geq 3$). $^{*}p < 0.05$, $^{***}p < 0.001$. (**C**) Viability assay. Resting and activated neutrophils were cultured in the presence and absence of KE-86-QG38 (10 μM), talabostat (50 μM), alogliptin (10 or 50 μM), and saxagliptin (10 or 50 μM). Neutrophils were cultured for 24 h before cell death analysis. All values are mean ± SEM ($n \geq 3$). $^{**}p < 0.01$, $^{***}p < 0.001$. (**D**) Viability assay. Resting and activated neutrophils were cultured in the presence and absence of M83 (1, 10, 50, 100, 200, 500, or 1000 μM). Neutrophils were cultured for 24 h before cell death analysis. All values are mean ± SEM ($n \geq 3$). $^{*}p < 0.05$.

prevented CD44-triggered ROS production (Fig. 3A, right panel) (31). Taken together, these data suggest that FAP-α activity is required for NOX activation following CD44 ligation of GM-CSF–primed human neutrophils.

FAP-α is a serine protease located as a dimer on the cell surface (14–16, 27) but can also occur in a soluble form in the cytoplasm (Fig. 2F) (15, 20, 25, 26). To investigate which FAP-α form is involved in the activation of the NOX, we used M83, a pseudopeptide FAP-α inhibitor shown to rapidly and completely block the proteolytic activity of FAP-α on the cell surface (25, 44, 52). M83 is charged and hydrophilic, thereby minimizing intracellular entry (52). M83 inhibited CD44-triggered ROS production in GM-CSF–primed neutrophils in a concentration-dependent manner (Fig. 3B). However, relatively high concentrations of M83 are required, and the overall efficacy is reduced as compared with KE-86-QG38 and TPCK (Fig. 3B). Moreover, only high concentrations of M83 were able to block CD44-triggered neutrophil death (Fig. 1D). Therefore, it is likely that the soluble FAP-α in the cytoplasm is the major FAP-α form involved in the signaling cascade, resulting in NOX activation and cell death.

Table I. The inhibitory effects of KE-86-QG38, alogliptin, and saxagliptin on the DPP4 gene family and unrelated DPP4-like proteases

	KE-86-QG38	Alogliptin	Saxagliptin
DPP4 IC_{50} (μM)	0.007 ± 0.0 (n = 2)	0.0041 ± 0.0029 (n = 12)	0.0046 ± 0.0008 (n = 12)
DPP2 IC_{50} (μM)	0.3 ± 0.0 (n = 2)	>30 (n = 2)	>30 (n = 8)
DPP8 IC_{50} (μM)	1.05 ± 0.07 (n = 2)	>30 (n = 6)	0.420 ± 0.348 (n = 8)
DPP9 IC_{50} (μM)	1.1 ± 0.0 (n = 2)	>30 (n = 6)	0.120 ± 0.070 (n = 8)
hPEP IC_{50} (μM)	>30 (n = 2)	>30 (n = 2)	>30 (n = 6)
hFAP-α IC_{50} (μM)	0.1 ± 0.0 (n = 2)	>30 (n = 2)	34.1 ± 22.7 (n = 8)

The structural formulae of the inhibitors are shown in Supplemental Fig. 1.
hPEP, human PEP; hFAP-α, human FAP-α.

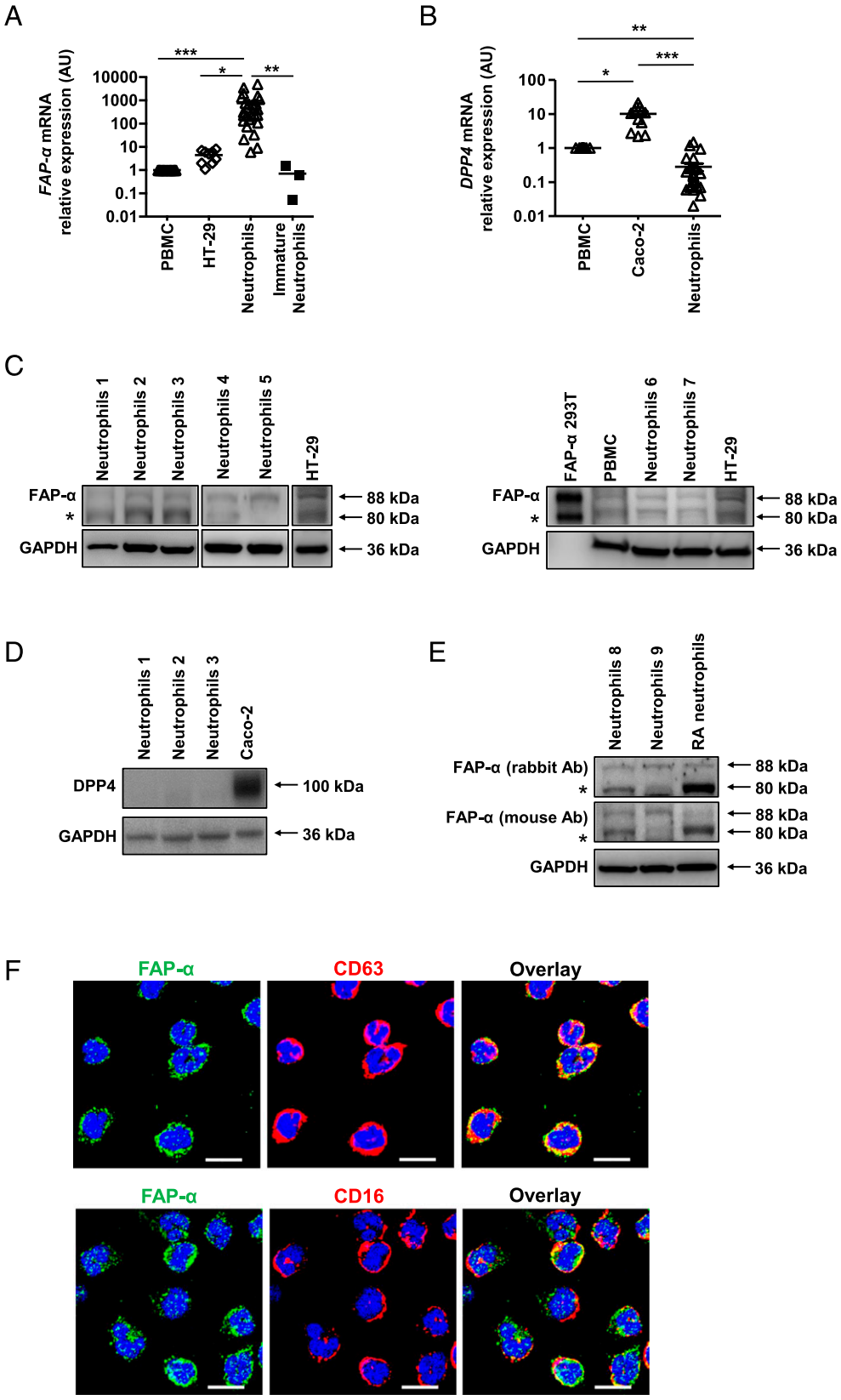

FIGURE 2. FAP-α is expressed by mature human neutrophils. (**A**) Quantitative PCR (qPCR) assay. Total RNA of PBMC, HT-29 cells, neutrophils, or immature neutrophils were isolated and *FAP-α* mRNA expression was analyzed by qPCR. Values are mean ± SEM ($n \geq 3$). *$p < 0.05$, **$p < 0.01$, ***$p < 0.001$. (**B**) qPCR assay. Total RNA of neutrophils, PBMC, or Caco-2 cells was isolated and *DPP4* mRNA expression was analyzed by qPCR. Values are mean ± SEM ($n \geq 9$). *$p < 0.05$, **$p < 0.01$, ***$p < 0.001$. (**C**) Immunoblotting. Neutrophil lysates from seven different donors were analyzed for FAP-α protein expression using mouse anti–FAP-α mAb 1E5. Five nanograms of FAP-α 293T cell–transient overexpression lysate was used as a positive control. We also analyzed cell lysates from PBMC and HT-29 cells. The lower band at ~80 kDa likely represents soluble FAP-α expression (labeled with *). GAPDH expression levels were analyzed as loading controls. Representative immunoblots are shown ($n \geq 3$). (**D**) Immunoblotting. Neutrophil lysates from three different donors were analyzed for DPP4 protein expression. A cell lysate from Caco-2 cells served as a *(Figure legend continues)*

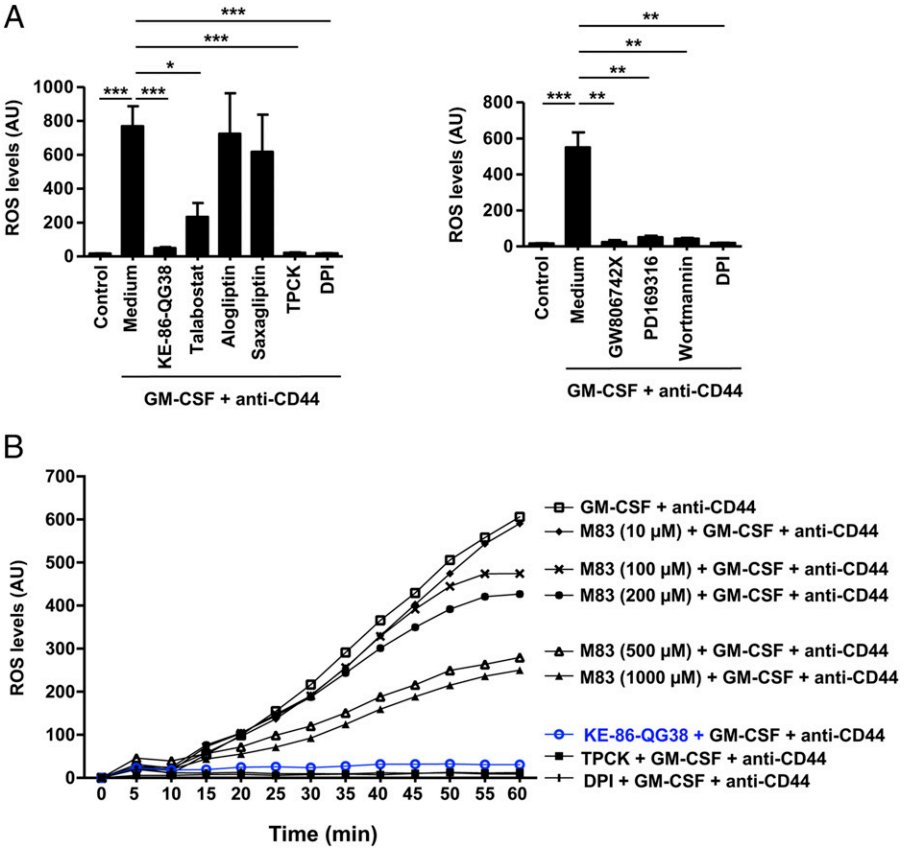

FIGURE 3. Enzymatic inhibition of FAP-α prevents CD44-triggered ROS production in GM-CSF–primed neutrophils. (**A**) DHR oxidation assay. Left, GM-CSF–primed neutrophils were precultured in the presence or absence of KE-86-QG38 (10 μM), talabostat (50 μM), alogliptin (10 μM), saxagliptin (10 μM), TPCK (10 μM), or DPI (1 μM) for 30 min and subsequently stimulated with anti-CD44 mAb for 15 min. Right, GM-CSF–primed neutrophils were precultured in the presence and absence of GW806742X (5 μM), PD169316 (10 μM), wortmannin (100 nM), or DPI (1 μM) for 30 min and subsequently stimulated with anti-CD44 mAb for 15 min. Values are mean ± SEM ($n \geq 4$). *$p < 0.05$, **$p < 0.01$, ***$p < 0.001$. (**B**) DHR oxidation assay. GM-CSF–primed neutrophils were precultured with M83 (10, 100, 200, 500, or 1000 μM), KE-86-QG38 (10 μM), TPCK (10 μM), or DPI (1 μM) for 30 min and subsequently stimulated with anti-CD44 mAb in a time-dependent manner. Data are representative of three independent experiments. One hour of PMA (25 μM) stimulation was used as a positive control and resulted in mean fluorescence intensity levels of 1721.

FAP-α activity is not required for RIPK3–MLKL–mediated p38 MAPK activation but regulates PI3K activity proximal to ROS production

To gain additional insight into the signaling events leading to the ROS formation, we next addressed the question whether FAP-α inhibition by KE-86-QG38 modulates the activities of p38 MAPK and PI3K, signaling events known to be proximal to ROS production in CD44-triggered neutrophil necroptosis (30, 31). The presence of KE-86-QG38 did not block p38 MAPK activation but completely prevented AKT phosphorylation (Fig. 4A). TPCK and talabostat also inhibited AKT phosphorylation (Supplemental Fig. 5). Wortmannin and PD169316 were used as controls in these experiments. To exclude the possibility that KE-86-QG38 directly blocks PI3K activity, we performed an in vitro PI3K activity assay. Although KE-86-QG38 was unable to block the production of PIP3 up to a concentration of 20 μM, PI-103, a PI3K inhibitor, blocked PI3K activity. As expected, wortmannin also blocked the PIP3 production in a concentration-dependent manner (Fig. 4B).

Moreover, we tested whether wortmannin was able to block the FAP-α enzyme; this is not the case (Fig. 4C). In contrast, KE-86-QG38 blocked the enzymatic activity of FAP-α in a concentration-dependent manner, confirming that it represents an effective pharmacological inhibitor of FAP-α. In contrast, the two DPP4 inhibitors alogliptin and saxagliptin had either no effect or partially blocked FAP-α activity (Fig. 4C). The partial inhibitory effect of saxagliptin (10 μM) is in agreement with its lower specificity as compared with alogliptin (Table I). It should be noted that TPCK also blocked FAP-α activity only partially (Fig. 4C).

These data suggested that KE-86-QG38 blocked the activity of PI3K in an indirect manner. The DPP4 inhibitors alogliptin and saxagliptin were not able to block PI3K activity (Fig. 4D). In contrast, GSK′843, a RIPK3 inhibitor, and GW806742X blocked both p38 MAPK and PI3K activation, as previously reported (Fig. 4D) (31). Collectively these data suggest that both FAP-α and p38 MAPK are proximal to PI3K activation. Although RIPK3 and MLKL are involved in p38 MAPK activation, FAP-α appears not to be involved in this process.

Interestingly, whereas PMA-induced ROS production cannot be inhibited by GW806742X, PD169316, or wortmannin (Fig. 4E, left), KE-86-QG38 and TPCK are able to completely block it (Fig. 4E, right). These data support the assumption that the induction of FAP-α activity occurs independently of the RIPK3–MLKL–p38 MAPK axis, confirming the data observed by immunoblotting in GM-CSF–primed and CD44-activated human neutrophils (Fig. 4A, 4D).

FAP-α activity is required for CD44-triggered ROS production and death in in vivo– primed human neutrophils

In agreement with previously published work (32), CD44 triggered high ROS production and subsequent cell death in neutrophils derived from joint fluids but not blood of RA patients in the absence of cytokine priming (Fig. 5A, 5B), suggesting that

positive control. GAPDH expression levels were analyzed as loading controls. Representative immunoblots are shown ($n \geq 3$). (**E**) Immunoblotting. Cell lysates from blood and joint fluid neutrophils were analyzed for FAP-α protein expression using rabbit anti–FAP-α Ab (upper) or mouse anti–FAP-α mAb 1E5 (lower). The lower band at ∼80 kDa may represent soluble FAP-α expression (labeled with *). GAPDH expression levels were analyzed as loading controls. Representative immunoblots are shown ($n \geq 3$). (**F**) Confocal microscopy. FAP-α was costained with CD63 (upper) and CD16 (lower) in freshly isolated human neutrophils. Scale bar, 10 μm. Images are representative of three independent experiments.

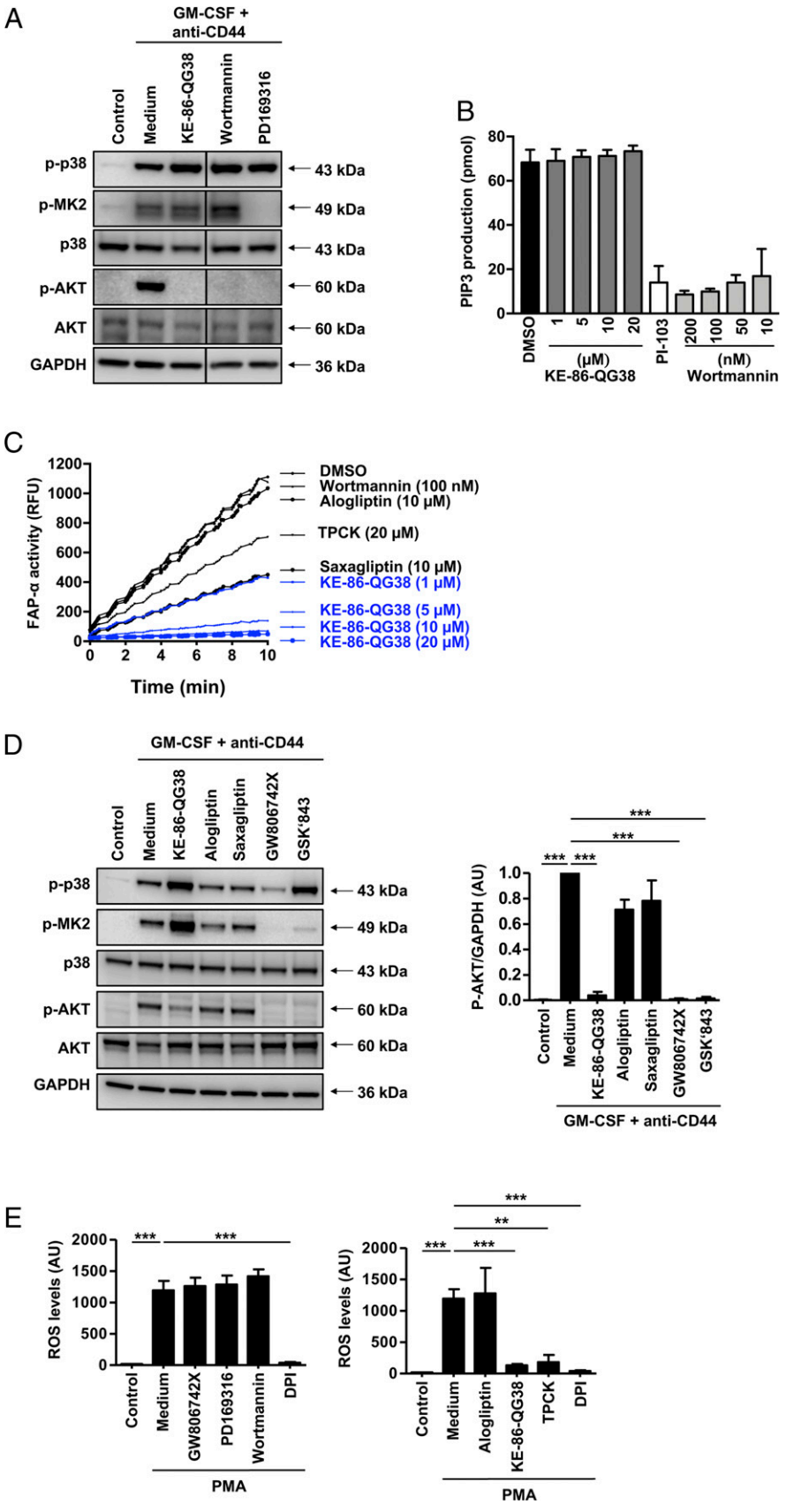

FIGURE 4. Enzymatic inhibition of FAP-α but not of DPP4 inhibits AKT phosphorylation following GM-CSF/CD44 activation and blocks PMA-stimulated ROS production in human neutrophils. (**A**) Immunoblotting. GM-CSF–primed neutrophils were cultured in the presence or absence of the indicated inhibitors (same concentrations as indicated in Fig. 3A) for 30 min and subsequently stimulated with anti-CD44 mAb for 15 min. Cell lysates were analyzed for p-p38, p-MK2, and p-AKT. As controls, we determined p38, AKT, and GAPDH expression levels. Representative immunoblots are shown ($n \geq 3$). (**B**) PI3K activity assay. In vitro enzymatic activity of PI3K was measured in the presence or absence of the indicated inhibitors, and the amount of PIP3 produced was quantified. Values are mean ± SEM ($n = 3$). (**C**) FAP-α activity assay. In vitro enzymatic activity of FAP-α was measured in the presence or absence of the indicated inhibitors and the relative fluorescent intensity was quantified. Data are representative of three independent experiments. (**D**) Left, Immunoblotting. GM-CSF–primed neutrophils were cultured in the presence or absence of the indicated inhibitors (same concentrations as indicated in Fig. 3A) for 30 min and subsequently stimulated with anti-CD44 mAb for 15 min. Cell lysates were analyzed for p-p38, p-MK2, and p-AKT. As controls, we determined p38, AKT, and GAPDH expression levels. As reported previously (31), pharmacological inactivation of RIPK3 or MLKL prevented both p38 MAPK and PI3K activation. Representative immunoblots are shown ($n \geq 3$). Right, p-AKT protein expression levels were quantified relative to the control condition of GAPDH. Values are mean ± SEM ($n \geq 3$). $^{***}p < 0.001$. (**E**) DHR oxidation assay. PMA-stimulated human neutrophils were precultured in the presence or absence of the indicated inhibitors (same concentrations as indicated in Fig. 3A) for 30 min and subsequently stimulated with PMA for 60 min. Values are mean ± SEM ($n \geq 3$). $^{**}p < 0.01$, $^{***}p < 0.001$.

joint fluid neutrophils were primed under in vivo conditions. Pharmacological inactivation of both FAP-α and RIPK3/MLKL by KE-86-QG38 and GSK′843/GW806742X, respectively, blocked CD44-triggered ROS production and cell death of joint fluid RA neutrophils (Fig. 5C, 5D, Supplemental Fig. 6), confirming the essential roles of these molecules in this nonapoptotic death pathway in inflammatory neutrophils of RA patients (Fig. 6).

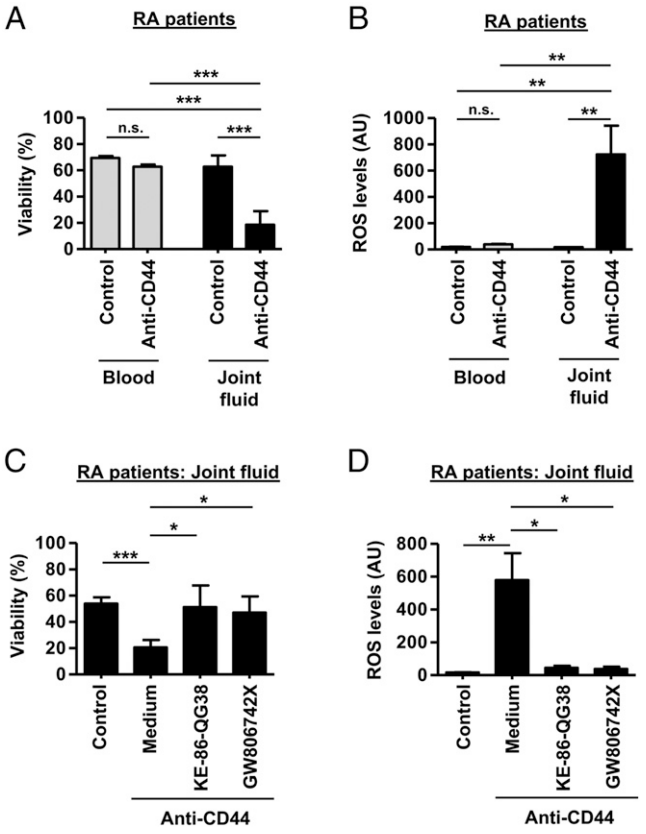

FIGURE 5. Enzymatic inhibition of FAP-α prevents CD44-triggered and cytokine priming-independent ROS production and cell death in joint fluid neutrophils derived from RA patients. (**A**) Viability assay. Blood and joint fluid neutrophils were cultured as indicated for 24 h in the absence of cytokine priming. Values are mean ± SEM ($n \geq 3$). (**B**) DHR oxidation assay. Blood and joint fluid neutrophils were cultured as indicated for 15 min in the absence of cytokine priming. Values are mean ± SEM ($n \geq 3$). (**C**) Viability assay. Joint fluid neutrophils were precultured in the presence or absence of KE-86-QG38 (10 μM) or GW806742X (5 μM) for 30 min and subsequently stimulated with anti-CD44 mAb for 24 h. Values are mean ± SEM ($n \geq 3$). (**D**) DHR oxidation assay. Joint fluid neutrophils were precultured in the presence and absence of KE-86-QG38 (10 μM) or GW806742X (5 μM) for 30 min and subsequently stimulated with anti-CD44 mAb for 15 min. Values are mean ± SEM ($n \geq 4$). $^*p < 0.05$, $^{**}p < 0.01$, $^{***}p < 0.001$.

Discussion

It has been previously shown that multiple triggers can induce a nonapoptotic death in cytokine-primed human neutrophils, which use components of the necroptotic death pathway (5, 30–33). This pathway results in the activation of the NOX, leading to the production of high levels of ROS that are a prerequisite for the nonapoptotic cell death to occur. Pharmacological or genetic inactivation of the NOX completely prevents neutrophil death (5, 30–33). For the activation of the NOX, it has been demonstrated that RIPK3 and MLKL are important proximal signaling molecules (31). In this study, we identified the serine protease FAP-α as an additional critical component that is activated after CD44 ligation in cytokine-primed human neutrophils.

In contrast to classical necroptosis, in CD44-triggered neutrophil necroptosis, MLKL is not involved in a pore-forming mechanism within the plasma membrane (5, 31). Rather, MLKL acts as an adaptor-like protein within a signaling cascade leading to p38 MAPK and PI3K activation, followed by the production of high levels of ROS (31). However, the proximal signaling events of RIPK3–MLKL activation remain to be determined. Following the initial observation that TPCK, a general serine protease inhibitor, is able to block CD44-induced ROS production and subsequent cell death, we used a pharmacological approach to identify the location of the serine protease in the pathway and to potentially identify it. We obtained evidence that FAP-α is required for both PI3K and NOX, but it did not affect the RIPK3–MLKL–p38 MAPK cascade. The assumption of a parallel activation of FAP-α independent of RIPK3–MLKL–p38 MAPK signaling is supported by the fact that PMA-stimulated ROS production is also blocked by enzymatic FAP-α inhibition but not by inhibitors of RIPK3 and MLKL (Fig. 6). Because TPCK blocked FAP-α activity partially only, we cannot exclude that, besides FAP-α, additional serine proteases are involved in CD44-induced ROS production.

FAP-α is a cell surface serine protease and is known as a 95-kDa type II integral membrane glycoprotein (14, 16, 27). In contrast, M83, an inhibitor known to block surface FAP-α had little efficacy only, suggesting that soluble FAP-α is largely responsible for PI3K and NOX activation (Fig. 6). It has been reported that FAP-α expression is not restricted to the cell membrane and substantial intracellular FAP-α can also be detected within the cells (15, 20, 25, 26). We obtained evidence for a soluble form of FAP-α in neutrophils by immunoblotting and confocal microscopy.

In resting neutrophils, the NOX is inactive, and its components are located in the cytoplasm as well as in cell and granule membranes (6). When neutrophils are activated, the cytoplasmic components of the NOX migrate to granule (>80%) and plasma cell membranes (~5%) (53), where they associate with the membrane-bound components to assemble the catalytically active enzyme (6). Therefore, it is possible that in CD44-induced neutrophil death, apart from membrane-bound FAP-α, soluble FAP-α may largely activate PI3K on the granule membranes to trigger ROS production or to facilitate cytosolic components of NOX directly to assemble the catalytically active enzyme on the membrane-bound components (Fig. 6). In this study, we have obtained evidence that a proportion of FAP-α is localized in close proximity to CD63 that is known to be expressed in azurophilic granules (51). Clearly, additional experimental work would be required to better understand the location and function of FAP-α in this nonapoptotic death pathway.

The NOXs enzyme family comprises NOX1, NOX2, NOX3, NOX4, NOX5, DUOX1, and DUOX2 isoforms. These enzyme isoforms share conserved structural properties and are all dedicated to ROS generation (54–56). Interestingly, DPP4 has been shown to bind directly with NOX1, which is crucial for lipid peroxidation and subsequent ferroptosis induced by erastin in TP53-deficient colorectal cancer cells (57). Because of its structural homology to DPP4, it is possible that FAP-α also interacts with NOX directly, most likely with NOX2 (58). Therefore, we cannot exclude that FAP-α also directly activates the NOX in neutrophils (Fig. 6).

It has been widely reported that FAP-α can activate cell signaling independent of its catalytic activity (20). For instance, FAP-α can form heteromeric complexes with DPP4 that are involved in many biological functions of cancer cells such as differentiation, growth, adhesion, and metastasis (16, 27, 59). In neutrophils, however, FAP-α proteolytic activity is required, and DPP4 is not expressed, excluding the possibility that FAP-α/DPP4 complexes are involved in the necroptotic signaling cascade.

In this study, we have also investigated the role of FAP-α in neutrophils derived from joint fluids of RA patients. CD44 ligation triggered cell death in these cells without the need of in vitro cytokine priming. Pharmacological inactivation of FAP-α prevented

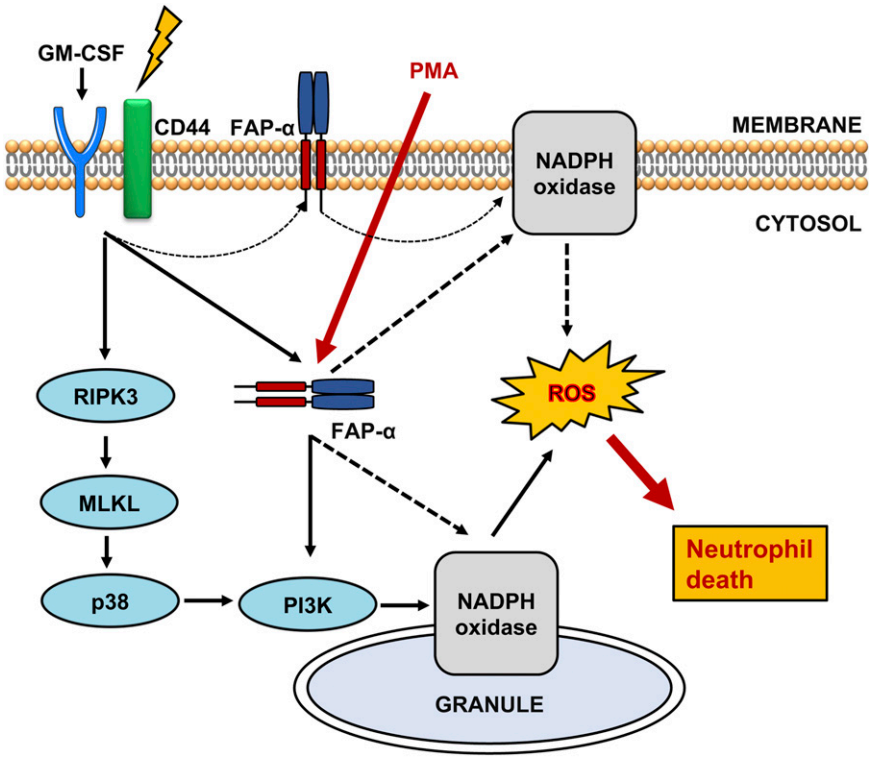

FIGURE 6. Schematic diagram showing the molecular pathway of a programmed nonapoptotic cell death in cytokine-primed human neutrophils. Ligation of adhesion receptors, including CD44, can induce cell death involving the RIPK3–MLKL–p38 MAPK–PI3K axis, in which all of these molecular components are prerequisite for generation of ROS induced by NOX. At the same time, the serine protease FAP-α activates PI3K independently and synergistically together with p38 MAPK. PMA-induced ROS production and subsequent nonapoptotic cell death also require FAP-α but is independent of the RIPK3–MLKL–p38 MAPK axis. The proximal events leading to RIPK3 and FAP-α activation remain to be determined.

CD44-induced ROS production and subsequent cell death in these cells, implying that FAP-α activity may accelerate inflammation by mediating an inflammatory neutrophil death in RA. A CD44-triggered neutrophil death pathway has been suggested to be involved in additional neutrophil-associated disorders such as cutaneous vasculitis, ulcerative colitis, and psoriasis (5, 30, 31). Therefore, identifying the key proteins, controlling ROS production, and subsequent nonapoptotic neutrophil death induced by adhesion molecules will provide novel drug targets for the treatment of neutrophil-associated disorders such as infectious, inflammatory, and autoimmune diseases.

In summary, we identified FAP-α, a serine protease, as a potential drug target in neutrophil-associated disorders. FAP-α activity is required for CD44-triggered ROS production and subsequent nonapoptotic cell death not only in GM-CSF–primed neutrophils of healthy donors, but also in inflammatory neutrophils without the need of in vitro cytokine priming. We provide evidence that it is the presence of cytoplasmic FAP-α that is required for triggering cell death. It should be noted that some DPP4 inhibitors, such as talabostat, which are already in preclinical trials or have been granted Food and Drug Administration approval for diseases, including cancer and type 2 diabetes mellitus (14, 19), might also be efficient in neutrophil-associated diseases, owing to their concurrent inhibition of FAP-α activity. In contrast, the natural substrates of FAP-α are not well identified (27). Thus, future studies should be conducted to identify the FAP-α binding partners in neutrophils and, perhaps, additional cell types.

Acknowledgments

We thank the participating patients and healthy blood donors for providing blood and joint fluid samples. Images were acquired on equipment supported by the Microscopy Imaging Centre at the University of Bern. The authors dedicate this work to the memory of Dr. Remo Perozzo.

Disclosures

The authors have no financial conflicts of interest.

References

1. Simon, H. U. 2003. Neutrophil apoptosis pathways and their modifications in inflammation. *Immunol. Rev.* 193: 101–110.
2. Nauseef, W. M., and N. Borregaard. 2014. Neutrophils at work. *Nat. Immunol.* 15: 602–611.
3. Cowland, J. B., and N. Borregaard. 2016. Granulopoiesis and granules of human neutrophils. *Immunol. Rev.* 273: 11–28.
4. Yousefi, S., D. Stojkov, N. Germic, D. Simon, X. Wang, C. Benarafa, and H. U. Simon. 2019. Untangling "NETosis" from NETs. *Eur. J. Immunol.* 49: 221–227.
5. Wang, X., S. Yousefi, and H. U. Simon. 2018. Necroptosis and neutrophil-associated disorders. *Cell Death Dis.* 9: 111.
6. Geering, B., and H. U. Simon. 2011. Peculiarities of cell death mechanisms in neutrophils. *Cell Death Differ.* 18: 1457–1469.
7. Geering, B., C. Stoeckle, S. Conus, and H. U. Simon. 2013. Living and dying for inflammation: neutrophils, eosinophils, basophils. *Trends Immunol.* 34: 398–409.
8. Hedstrom, L. 2002. Serine protease mechanism and specificity. *Chem. Rev.* 102: 4501–4524.
9. Heutinck, K. M., I. J. ten Berge, C. E. Hack, J. Hamann, and A. T. Rowshani. 2010. Serine proteases of the human immune system in health and disease. *Mol. Immunol.* 47: 1943–1955.
10. Turk, B., D. Turk, and V. Turk. 2012. Protease signalling: the cutting edge. *EMBO J.* 31: 1630–1643.
11. Soualmia, F., and C. El Amri. 2018. Serine protease inhibitors to treat inflammation: a patent review (2011-2016). *Expert Opin. Ther. Pat.* 28: 93–110.
12. Park, J. E., M. C. Lenter, R. N. Zimmermann, P. Garin-Chesa, L. J. Old, and W. J. Rettig. 1999. Fibroblast activation protein, a dual specificity serine protease expressed in reactive human tumor stromal fibroblasts. *J. Biol. Chem.* 274: 36505–36512.
13. O'Brien, P., and B. F. O'Connor. 2008. Seprase: an overview of an important matrix serine protease. *Biochim. Biophys. Acta* 1784: 1130–1145.
14. Yazbeck, R., G. S. Howarth, and C. A. Abbott. 2009. Dipeptidyl peptidase inhibitors, an emerging drug class for inflammatory disease? *Trends Pharmacol. Sci.* 30: 600–607.
15. Hamson, E. J., F. M. Keane, S. Tholen, O. Schilling, and M. D. Gorrell. 2014. Understanding fibroblast activation protein (FAP): substrates, activities, expression and targeting for cancer therapy. *Proteomics Clin. Appl.* 8: 454–463.
16. Wagner, L., C. Klemann, M. Stephan, and S. von Hörsten. 2016. Unravelling the immunological roles of dipeptidyl peptidase 4 (DPP4) activity and/or structure homologue (DASH) proteins. *Clin. Exp. Immunol.* 184: 265–283.
17. Lay, A. J., H. E. Zhang, G. W. McCaughan, and M. D. Gorrell. 2019. Fibroblast activation protein in liver fibrosis. *Front. Biosci.* 24: 1–17.
18. Deacon, C. F. 2019. Physiology and pharmacology of DPP-4 in glucose homeostasis and the treatment of type 2 diabetes. [Published erratum appears in 2019 *Front. Endocrinol. (Lausanne)* 10: 275.] *Front. Endocrinol. (Lausanne)* 10: 80.
19. Waumans, Y., L. Baerts, K. Kehoe, A. M. Lambeir, and I. De Meester. 2015. The dipeptidyl peptidase family, prolyl oligopeptidase, and prolyl carboxypeptidase

in the immune system and inflammatory disease, including atherosclerosis. *Front. Immunol.* 6: 387.
20. Kelly, T., Y. Huang, A. E. Simms, and A. Mazur. 2012. Fibroblast activation protein-α: a key modulator of the microenvironment in multiple pathologies. *Int. Rev. Cell Mol. Biol.* 297: 83–116.
21. Narra, K., S. R. Mullins, H. O. Lee, B. Strzemkowski-Brun, K. Magalong, V. J. Christiansen, P. A. McKee, B. Egleston, S. J. Cohen, L. M. Weiner, et al. 2007. Phase II trial of single agent Val-boroPro (Talabostat) inhibiting fibroblast activation protein in patients with metastatic colorectal cancer. *Cancer Biol. Ther.* 6: 1691–1699.
22. Eager, R. M., C. C. Cunningham, N. Senzer, D. A. Richards, R. N. Raju, B. Jones, M. Uprichard, and J. Nemunaitis. 2009. Phase II trial of talabostat and docetaxel in advanced non-small cell lung cancer. *Clin. Oncol. (R. Coll. Radiol.)* 21: 464–472.
23. Eager, R. M., C. C. Cunningham, N. N. Senzer, J. Stephenson, Jr., S. P. Anthony, S. J. O'Day, G. Frenette, A. C. Pavlick, B. Jones, M. Uprichard, and J. Nemunaitis. 2009. Phase II assessment of talabostat and cisplatin in second-line stage IV melanoma. *BMC Cancer* 9: 263.
24. Kirby, M., D. M. Yu, S. O'Connor, and M. D. Gorrell. 2009. Inhibitor selectivity in the clinical application of dipeptidyl peptidase-4 inhibition. *Clin. Sci. (Lond.)* 118: 31–41.
25. Christiansen, V. J., K. W. Jackson, K. N. Lee, T. D. Downs, and P. A. McKee. 2013. Targeting inhibition of fibroblast activation protein-α and prolyl oligopeptidase activities on cells common to metastatic tumor microenvironments. *Neoplasia* 15: 348–358.
26. Mori, Y., K. Kono, Y. Matsumoto, H. Fujii, T. Yamane, M. Mitsumata, and W. T. Chen. 2004. The expression of a type II transmembrane serine protease (Seprase) in human gastric carcinoma. *Oncology* 67: 411–419.
27. Kelly, T. 2005. Fibroblast activation protein-alpha and dipeptidyl peptidase IV (CD26): cell-surface proteases that activate cell signaling and are potential targets for cancer therapy. *Drug Resist. Updat.* 8: 51–58.
28. Dolznig, H., N. Schweifer, C. Puri, N. Kraut, W. J. Rettig, D. Kerjaschki, and P. Garin-Chesa. 2005. Characterization of cancer stroma markers: in silico analysis of an mRNA expression database for fibroblast activation protein and endosialin. *Cancer Immun.* 5: 10.
29. Tchou, J., P. J. Zhang, Y. Bi, C. Satija, R. Marjumdar, T. L. Stephen, A. Lo, H. Chen, C. Mies, C. H. June, et al. 2013. Fibroblast activation protein expression by stromal cells and tumor-associated macrophages in human breast cancer. *Hum. Pathol.* 44: 2549–2557.
30. Mihalache, C. C., S. Yousefi, S. Conus, P. M. Villiger, E. M. Schneider, and H. U. Simon. 2011. Inflammation-associated autophagy-related programmed necrotic death of human neutrophils characterized by organelle fusion events. *J. Immunol.* 186: 6532–6542.
31. Wang, X., Z. He, H. Liu, S. Yousefi, and H. U. Simon. 2016. Neutrophil necroptosis is triggered by ligation of adhesion molecules following GM-CSF priming. *J. Immunol.* 197: 4090–4100.
32. von Gunten, S., S. Yousefi, M. Seitz, S. M. Jakob, T. Schaffner, R. Seger, J. Takala, P. M. Villiger, and H. U. Simon. 2005. Siglec-9 transduces apoptotic and nonapoptotic death signals into neutrophils depending on the proinflammatory cytokine environment. *Blood* 106: 1423–1431.
33. Wehrli, M., F. Cortinas-Elizondo, R. Hlushchuk, F. Daudel, P. M. Villiger, S. Miescher, A. W. Zuercher, V. Djonov, H. U. Simon, and S. von Gunten. 2014. Human IgA Fc receptor FcαRI (CD89) triggers different forms of neutrophil death depending on the inflammatory microenvironment. *J. Immunol.* 193: 5649–5659.
34. Altznauer, F., S. Martinelli, S. Yousefi, C. Thürig, I. Schmid, E. M. Conway, M. H. Schöni, P. Vogt, C. Mueller, M. F. Fey, et al. 2004. Inflammation-associated cell cycle-independent block of apoptosis by survivin in terminally differentiated neutrophils. *J. Exp. Med.* 199: 1343–1354.
35. Simon, D., S. Borelli, L. R. Braathen, and H. U. Simon. 2002. Peripheral blood mononuclear cells from IgE- and non-IgE-associated allergic atopic eczema/dermatitis syndrome (AEDS) demonstrate increased capacity of generating interleukin-13 but differ in their potential of synthesizing interferon-gamma. *Allergy* 57: 431–435.
36. Simon, D., L. R. Braathen, and H. U. Simon. 2007. Increased lipopolysaccharide-induced tumour necrosis factor-alpha, interferon-gamma and interleukin-10 production in atopic dermatitis. *Br. J. Dermatol.* 157: 583–586.
37. Geering, B., U. Gurzeler, E. Federzoni, T. Kaufmann, and H. U. Simon. 2011. A novel TNFR1-triggered apoptosis pathway mediated by class IA PI3Ks in neutrophils. *Blood* 117: 5953–5962.
38. Amini, P., D. Stojkov, A. Felser, C. B. Jackson, C. Courage, A. Schaller, L. Gelman, M. E. Soriano, J. M. Nuoffer, L. Scorrano, et al. 2018. Neutrophil extracellular trap formation requires OPA1-dependent glycolytic ATP production. *Nat. Commun.* 9: 2958.
39. Radonjic-Hoesli, S., X. Wang, E. de Graauw, C. Stoeckle, B. Styp-Rekowska, R. Hlushchuk, D. Simon, P. J. Spaeth, S. Yousefi, and H. U. Simon. 2017. Adhesion-induced eosinophil cytolysis requires the receptor-interacting protein kinase 3 (RIPK3)-mixed lineage kinase-like (MLKL) signaling pathway, which is counterregulated by autophagy. *J. Allergy Clin. Immunol.* 140: 1632–1642.
40. Conus, S., and H. U. Simon. 2008. Cathepsins: key modulators of cell death and inflammatory responses. *Biochem. Pharmacol.* 76: 1374–1382.
41. Benarafa, C., and H. U. Simon. 2017. Role of granule proteases in the life and death of neutrophils. *Biochem. Biophys. Res. Commun.* 482: 473–481.
42. Feng, J., Z. Zhang, M. B. Wallace, J. A. Stafford, S. W. Kaldor, D. B. Kassel, M. Navre, L. Shi, R. J. Skene, T. Asakawa, et al. 2007. Discovery of alogliptin: a potent, selective, bioavailable, and efficacious inhibitor of dipeptidyl peptidase IV. [Published erratum appears in 2008 *J. Med. Chem.* 51: 4357.] *J. Med. Chem.* 50: 2297–2300.
43. Augeri, D. J., J. A. Robl, D. A. Betebenner, D. R. Magnin, A. Khanna, J. G. Robertson, A. Wang, L. M. Simpkins, P. Taunk, Q. Huang, et al. 2005. Discovery and preclinical profile of Saxagliptin (BMS-477118): a highly potent, long-acting, orally active dipeptidyl peptidase IV inhibitor for the treatment of type 2 diabetes. *J. Med. Chem.* 48: 5025–5037.
44. Lee, K. N., K. W. Jackson, V. J. Christiansen, E. K. Dolence, and P. A. McKee. 2011. Enhancement of fibrinolysis by inhibiting enzymatic cleavage of precursor α2-antiplasmin. *J. Thromb. Haemost.* 9: 987–996.
45. Cao, F., S. Wang, H. Wang, and W. Tang. 2018. Fibroblast activation protein-α in tumor cells promotes colorectal cancer angiogenesis via the Akt and ERK signaling pathways. *Mol. Med. Rep.* 17: 2593–2599.
46. Darmoul, D., M. Lacasa, L. Baricault, D. Marguet, C. Sapin, P. Trotot, A. Barbat, and G. Trugnan. 1992. Dipeptidyl peptidase IV (CD 26) gene expression in enterocyte-like colon cancer cell lines HT-29 and Caco-2. Cloning of the complete human coding sequence and changes of dipeptidyl peptidase IV mRNA levels during cell differentiation. *J. Biol. Chem.* 267: 4824–4833.
47. Kim, K. M., J. H. Noh, M. Bodogai, J. L. Martindale, X. Yang, F. E. Indig, S. K. Basu, K. Ohnuma, C. Morimoto, P. F. Johnson, et al. 2017. Identification of senescent cell surface targetable protein DPP4. *Genes Dev.* 31: 1529–1534.
48. Lettau, M., M. Dietz, S. Vollmers, F. Armbrust, C. Peters, T. M. Dang, G. Chitadze, D. Kabelitz, and O. Janssen. 2020. Degranulation of human cytotoxic lymphocytes is a major source of proteolytically active soluble CD26/DPP4. *Cell. Mol. Life Sci.* 77: 751–764.
49. Lai, D., L. Ma, and F. Wang. 2012. Fibroblast activation protein regulates tumor-associated fibroblasts and epithelial ovarian cancer cells. *Int. J. Oncol.* 41: 541–550.
50. Chung, K. M., S. C. Hsu, Y. R. Chu, M. Y. Lin, W. T. Jiaang, R. H. Chen, and X. Chen. 2014. Fibroblast activation protein (FAP) is essential for the migration of bone marrow mesenchymal stem cells through RhoA activation. *PLoS One* 9: e88772.
51. Cham, B. P., J. M. Gerrard, and D. F. Bainton. 1994. Granulophysin is located in the membrane of azurophilic granules in human neutrophils and mobilizes to the plasma membrane following cell stimulation. *Am. J. Pathol.* 144: 1369–1380.
52. Jackson, K. W., V. J. Christiansen, V. R. Yadav, R. Silasi-Mansat, F. Lupu, V. Awasthi, R. R. Zhang, and P. A. McKee. 2015. Suppression of tumor growth in mice by rationally designed pseudopeptide inhibitors of fibroblast activation protein and prolyl oligopeptidase. *Neoplasia* 17: 43–54.
53. Sengeløv, H., M. H. Nielsen, and N. Borregaard. 1992. Separation of human neutrophil plasma membrane from intracellular vesicles containing alkaline phosphatase and NADPH oxidase activity by free flow electrophoresis. *J. Biol. Chem.* 267: 14912–14917.
54. Bedard, K., and K. H. Krause. 2007. The NOX family of ROS-generating NADPH oxidases: physiology and pathophysiology. *Physiol. Rev.* 87: 245–313.
55. Brown, D. I., and K. K. Griendling. 2009. Nox proteins in signal transduction. *Free Radic. Biol. Med.* 47: 1239–1253.
56. Magnani, F., S. Nenci, E. Millana Fananas, M. Ceccon, E. Romero, M. W. Fraaije, and A. Mattevi. 2017. Crystal structures and atomic model of NADPH oxidase. *Proc. Natl. Acad. Sci. USA* 114: 6764–6769.
57. Xie, Y., S. Zhu, X. Song, X. Sun, Y. Fan, J. Liu, M. Zhong, H. Yuan, L. Zhang, T. R. Billiar, et al. 2017. The tumor suppressor p53 limits ferroptosis by blocking DPP4 activity. *Cell Rep.* 20: 1692–1704.
58. Winterbourn, C. C., A. J. Kettle, and M. B. Hampton. 2016. Reactive oxygen species and neutrophil function. *Annu. Rev. Biochem.* 85: 765–792.
59. Ghersi, G., H. Dong, L. A. Goldstein, Y. Yeh, L. Hakkinen, H. S. Larjava, and W. T. Chen. 2002. Regulation of fibroblast migration on collagenous matrix by a cell surface peptidase complex. *J. Biol. Chem.* 277: 29231–29241.